Atmospheric Environment 108 (2015) 20–31

Contents lists available at ScienceDirect

Atmospheric Environment

journal homepage: www.elsevier.com/locate/atmosenv

Characteristics of flow and reactive pollutant dispersion in urban street canyons

Soo-Jin Park [a], Jae-Jin Kim [a,*], Minjoong J. Kim [b], Rokjin J. Park [b], Hyeong-Bin Cheong [a]

[a] Department of Environmental Atmospheric Sciences, Pukyong National University, Busan, South Korea
[b] School of Earth and Environmental Sciences, Seoul National University, Seoul, South Korea

HIGHLIGHTS

- We investigate the characteristics of flow and reactive pollutant dispersion in street canyons.
- Near the street bottom, there is a marked difference in flow pattern between in shallow and deep street canyons.
- O_3 concentration near the street bottom depends on street-canyon aspect ratio.
- In deep street canyons, canyon-height increase results in an increase (decrease) in averaged NO_X (O_3) concentration.
- At high VOC–NO_X ratios, O_3 is formed through the photolysis of NO_2 by VOC degradation reactions.

ARTICLE INFO

Article history:
Received 13 November 2014
Accepted 26 February 2015
Available online 26 February 2015

Keywords:
CFD-chemistry-coupled model
Reactive pollutants
Street canyon
Aspect ratio
VOC–NO_X ratio

ABSTRACT

In this study, the effects of aspect ratio defined as the ratio of building height to street width on the dispersion of reactive pollutants in street canyons were investigated using a coupled CFD-chemistry model. Flow characteristics for different aspect ratios were analyzed first. For each aspect ratio, six emission scenarios with different VOC–NO_X ratios were considered. One vortex was generated when the aspect ratio was less than 1.6 (shallow street canyon). When the aspect ratio was greater than 1.6 (deep street canyon), two vortices were formed in the street canyons. Comparing to previous studies on two-dimensional street canyons, the vortex center is slanted toward the upwind building and reverse and downward flows are dominant in street canyons. Near the street bottom, there is a marked difference in flow pattern between in shallow and deep street canyons. Near the street bottom, reverse and downward flows are dominant in shallow street canyon and flow convergence exists near the center of the deep street canyons, which induces a large difference in the NO_X and O_3 dispersion patterns in the street canyons. NO_X concentrations are high near the street bottom and decreases with height. The O_3 concentrations are low at high NO concentrations near the street bottom because of NO titration. At a low VOC–NO_X ratio, the NO concentrations are sufficiently high to destroy large amount of O_3 by titration, resulting in an O_3 concentration in the street canyon much lower than the background concentration. At high VOC–NO_X ratios, a small amount of O_3 is destroyed by NO titration in the lower layer of the street canyons. However, in the upper layer, O_3 is formed through the photolysis of NO_2 by VOC degradation reactions. As the aspect ratio increases, NO_X (O_3) concentrations averaged over the street canyons decrease (increase) in the shallow street canyons. This is because outward flow becomes strong and NO_X flux toward the outsides of the street canyons increases, resulting in less NO titration. In the deep street canyons, outward flow becomes weak and outward NO_X flux decreases, resulting in an increase (decrease) in NO_X (O_3) concentration.

1. Introduction

Urbanization has provided humans and their properties to be exposed to threats and damage from hazardous pollutants. One of the most important causes is increased pollutant emission caused by the growth in traffic and the associated congestion. Another

* Corresponding author. Department of Environmental Atmospheric Sciences, Pukyong National University, 599-1, Daeyeon 3-Dong, Nam-Gu, 608-737 Busan, South Korea.
E-mail address: jjkim@pknu.ac.kr (J.-J. Kim).

http://dx.doi.org/10.1016/j.atmosenv.2015.02.065
1352-2310/

cause is the deterioration of the pollutant-ventilation environment resulting from the construction of high-rise buildings and the increase in building density.

Many previous studies (Chan et al., 2002; Jeong and Andrews, 2002; Sagrado et al., 2002; Assimakopoulos et al., 2003; Chang and Meroney, 2003; Park et al., 2004; Kang et al., 2008; Kim and Baik, 2010; Tominaga and Stathopoulos, 2010; Yoshie et al., 2011; Kikumoto and Ooka, 2012) have investigated the characteristics of flow and dispersion in urban areas. Although various types of building configuration exist in real urban areas, idealized building configurations (i.e., single obstacle and street-canyon) have been taken into account in most previous studies to understand the basic mechanisms of dynamic and dispersion processes. Based on previous studies, the important factors affecting flow patterns and the associated dispersion of passive scalar pollutants can be placed into the following three categories: inflow conditions, such as wind speed/direction (Chan et al., 2002; Kim and Baik, 2004; Park et al., 2004) and turbulence intensity (Tominaga and Stathopoulos, 2010; Yoshie et al., 2011; Kikumoto and Ooka, 2012); geometric conditions of building configuration, such as building aspect ratio (Jeong and Andrews, 2002; Sagrado et al., 2002; Assimakopoulos et al., 2003) and street-canyon aspect ratio (Chang and Meroney, 2003; Liu et al., 2004); and ground- and building-surface conditions, such as surface roughness and surface heating/cooling (Meroney et al., 1996; Kang et al., 2008; Kim and Baik, 2010; Kim et al., 2014).

The majority of previous studies have focused on the dispersion of passive scalar (nonreactive) pollutants (Sini et al., 1996; Kim and Baik, 2004; Liu et al., 2004; Baik et al., 2009; Yoshie et al., 2011; Li et al., 2012); however, pollutants emitted from vehicles are mostly reactive. The primary pollutants emitted from vehicles in street canyons are volatile organic compounds (VOCs) and nitrogen oxides ($NO_X = NO + NO_2$). These compounds chemically react with each other to produce toxic secondary pollutants including ozone (O_3) and aerosols, which are major concerns for air quality in urban areas (Weschler, 2006). The previous studies on air quality in urban street canyons (Baker et al., 2004; Baik et al., 2007; Grawe et al., 2007; Kang et al., 2008) contributed to the establishment of a basic framework for urban air-quality prediction. However, the steady-state O_3–NO–NO_2 photochemistry that those studies used does not include the reactions of important O_3 precursors (i.e., reactive VOCs) and is too simple for realistic simulations of the complex chemical processes in urban street canyons. Some studies (Garmory et al., 2009; Kwak and Baik, 2012) have considered more complex photochemical reactions with VOCs to simulate the dispersion of reactive pollutants. Garmory et al. (2009) found no significant difference in NO_X and O_3 concentrations between the Stochastic Fields method and CBM-IV chemical modules. Kim et al. (2012) revealed the importance of a full-chemistry simulation for air-quality modeling in urban street canyons using a coupled CFD-chemistry model with the full photochemical mechanism and online photolysis rate computation module.

In this study, we investigated the effects of street-canyon aspect ratio on the dispersion of reactive pollutants in urban street canyons with the coupled CFD-chemistry model used by Kim et al. (2012). For this, flow characteristics with different aspect ratios were first analyzed. For each aspect ratio, six emission scenarios with different VOC–NO_X ratios were considered and the characteristics of dispersion of reactive pollutants were analyzed.

2. Model description and simulation setup

2.1. Model description

The coupled CFD-chemistry model used in this study was that used by Kim et al. (2012). The CFD model based on the Reynolds-averaged Navier–Stokes equations (RANS) model. The model assumes a three-dimensional, nonhydrostatic, nonrotating, and Bussinesq airflow system and employs a k-ε turbulent closure scheme based on the renormalization group (RNG) theory. A full NO_X–O_X–VOCs chemical mechanism taken from the GEOS-Chem model developed by the Harvard University modeling group (Bey et al., 2001) was implemented in the CFD model for simulating chemical reactions of reactive species. In the chemistry module, a gear-type solver, Sparse Matrix Vectorized Gear Code (SMVGEAR) (Jacobson and Turco, 1994) calculates 293 chemical reactions and 50 photochemical reactions for 110 species. Using the CFD-Chemistry model with steady-state photochemistry, Kim et al. (2012) successfully reproduced the reactive pollutant distributions for the idealized street-canyon simulated by Baker et al. (2004). Also, Kim et al. (2012) showed that the developed CFD-chemistry model could be applicable to air-quality predictions in urban areas by comparing the values to field observations (Xie et al. 2003).

2.2. Simulation setup

Fig. 1 shows the computational domain and building configuration. The domain sizes (cell number) are 120 × 80 × 200 m (60 × 40 × 100) in the x, y, and z directions, respectively. The grid intervals in all directions are 2 m. For systematic variation of the street-canyon aspect ratio defined by the ratio of building height (H) to street width (S), building height is set to 20, 24, 28, 32, and 40 m and building length (L), building width (W) and street width are fixed at 20 m (Table 1). For simplicity, the spaces between the buildings in the x and y directions are respectively named the streamwise street and street canyon. The vertical profiles of ambient wind, turbulent kinetic energy (TKE) and TKE dissipation rate are given below (Castro and Apsley, 1997):

$$U(z) = \frac{u_*}{\kappa} \ln\left(\frac{z}{z_0}\right), \tag{1}$$

$$V(z) = 0, \tag{2}$$

$$W(z) = 0, \tag{3}$$

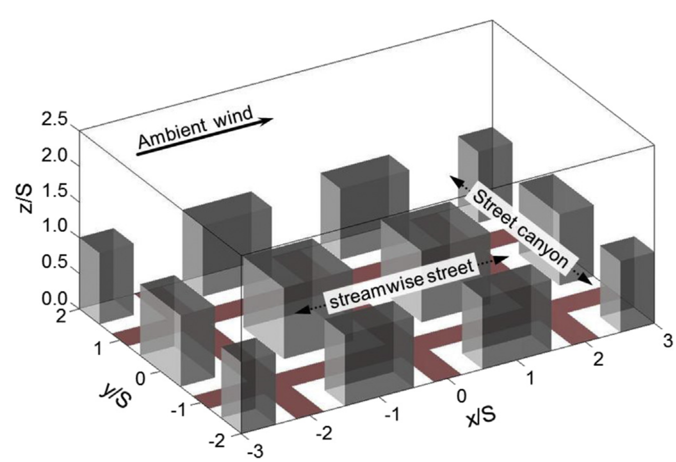

Fig. 1. The computational domain and building configuration. The red color at bottom indicates the line-type emission source. (For interpretation of the references to colour in this figure legend, the reader is referred to the web version of this article.)

Table 1
Summary of building configurations considered in this study.

Building height (m), H	Building width (m)	Building length (m)	Street width (m), S	Aspect ratio (H/S)
20	20	20	20	1.0
24	20	20	20	1.2
28	20	20	20	1.4
32	20	20	20	1.6
36	20	20	20	1.8
40	20	20	20	2.0

$$k(z) = \frac{u_*^2}{C_\mu^{1/2}}\left(1 - \frac{z}{\delta}\right)^2, \tag{4}$$

$$\varepsilon(z) = \frac{C_\mu^{3/4} k^{3/2}}{\kappa z}, \tag{5}$$

here, u_*, z_0 and κ are the friction velocity, roughness length (=0.05 m), and von Karman constant (=0.4), respectively. C_μ is an empirical constant (=0.0845). The ambient wind speed at 20 m is 6.05 m s^{-1}. The air temperature is set to 293 K (isothermal conditions).

For each aspect ratio, six scenarios with fixed VOC (=50 ppbv s^{-1}) but varied NO_X emissions are applied to investigate the effects of the VOC–NO_X ratio on the dispersion characteristics of primary and secondary pollutants in the street canyon (Table 2). The volumetric ratio of NO and NO_2 emission is 10:1 (Buckingham et al., 1997). The initialization method used in this study follows that of Baker et al. (2004) and Kim et al. (2012). In each emission scenario, the coupled CFD-chemistry model is integrated for 90 min with a time step of 0.1 s. For the first 30 min (t = 0–30 min) of model integration, there is no emission to establish a mean flow structure within the street canyon in the model domain. For the next 30 min (t = 30–60 min), passive (nonreactive) pollutants are emitted at the same rate as NO_X (Table 2) along line-type sources (Fig. 1), which represents emissions from an idealized traffic flow. The NO_X concentration at each grid cell is then equated to the passive pollutant concentration at t = 60 min and the ratio of NO and NO_2 concentrations at each grid cell is set to 10:1. After 60 min, NO and NO_2 are emitted at the rates for each scenario shown in Table 2. The background and initial O_3 concentrations are assumed to be 40 ppbv. The volumetric emission proportions of ALK4, PRPE, ethane, formaldehyde, propane, acetone, acetaldehyde, and RCHO are 45.41%, 37.95%, 6.51%, 3.98%, 2.46%, 1.85%, 1.08%, and 0.76%, respectively (Fraser and Cass, 1998; Schmid et al., 2001). The emission source with 1-m height and 12-m width in the computational domain is located at the center of the streamwise and street canyons (Fig. 1).

2.3. Model validation

Kim and Baik (2010) evaluated the CFD model used in this study with data from wind-tunnel experiments conducted by Uehara et al. (2000). The model successfully reproduced the vertical profiles of wind and temperature both with and without street-canyon bottom heating. Recently, Kim et al. (2012) developed a CFD-chemistry model by implementing a full NO_X–O_X–VOCs chemical mechanism from the GEOS-Chem model (Bey et al., 2001). The CFD-chemistry model was evaluated by comparing it with the large eddy simulation (LES) model results by Baker et al. (2004). The results were consistent with Baker et al. (2004). The CFD-chemistry model was also applied to observations by Xie et al. (2003). Despite its effective simulation of CO concentrations, the CFD-chemistry model reproduced NO_X and O_3 concentrations relatively poorly because of uncertainty in emissions and background information about primary and secondary pollutants.

To determine how the model simulates the transportation of pollutants emitted inside a street canyon, we evaluate the model performance for non-reactive tracer transport by comparing it with the previous wind-tunnel experiment conducted by Pavageau and Schatzmann (1999). In the aforementioned work, the non-dimensional concentration (K) was used and was defined by $CU_{ref}hl/Q$ (here, C, U_{ref}, h, and Q denote tracer concentration, velocity at a reference height, street-canyon height, and emission rate of line source with length of l, respectively). For comparison, the non-dimensional concentration (K) was divided by the mean concentration in the street canyon ($\overline{K}$). Fig. 2 shows a traditional dispersion pattern in a two-dimensional (infinitely long) street canyon. Concentrations are high near the upwind buildings due to reverse flow passing through the source near the street bottom; however, concentrations are low near the downwind building because of the intrusion of relatively clean air flow above the street canyon. The simulated concentrations show good agreement with the measured concentrations in their dispersion pattern, despite a small overestimation near the upwind region. Based on these results, the CFD-chemistry-coupled model is adequate for studying flow and dispersion in urban street canyons.

3. Results and discussion

3.1. Flow characteristics

We performed a number of experiments for different aspect ratios in three-dimensional street canyons with a fixed street width and different building heights and first analyzed the mean flow characteristics. Fig. 3 shows the streamline fields at y/S = 0.05 and the wind vector fields at z/S = 0.15. In the H/S = 1.0 case, one vortex appears vertically and the reverse and outward flows are dominant near the street bottom (Fig. 3a and c). The clockwise-rotating vortex results in the reverse flow in the lower layer and the center of the vortex is located near the upwind building in the upper layer. Previous studies of two-dimensional street canyons have shown that a roll-type vortex is generated and its center is located at the middle of the street canyon (Chan et al., 2002; Assimakopoulos et al., 2003; Baik et al., 2012). However, the center of the vortex in this study appears near the upwind building in the upper layer. Airflow coming from above and outside the street canyon converges near the downwind building and participates in the reverse flow. This resulted in the formation of a portal-type vortex in which the top part slanted toward the upwind building in the street canyon (Kim and Baik, 2004, 2010; Gowardhan et al., 2011).

In the H/S = 2.0 case, two counter-rotating vortices appear vertically in the street canyon. The primary (secondary) vortex rotating clockwise (counterclockwise) is formed in the upper (lower) layer. At the mid-layer of the street canyon (0.5 < z/S < 1.5), reverse and downward flows are dominant. The secondary vortex appears in the upwind half side (−0.5 < x/S < 0.0) of the lower layer

Table 2
Summary of the six emission scenarios considered in this study.

NO (ppb s^{-1})	NO_2 (ppb s^{-1})	NO_X (ppb s^{-1})	VOCs (ppb s^{-1})	VOC–NO_X ratio
45.45	4.55	50.00	50.0	1.0
22.73	2.27	25.00	50.0	2.0
11.36	1.14	12.50	50.0	4.0
7.55	0.75	8.30	50.0	6.0
5.68	0.57	6.25	50.0	8.0
4.55	0.45	5.00	50.0	10.0

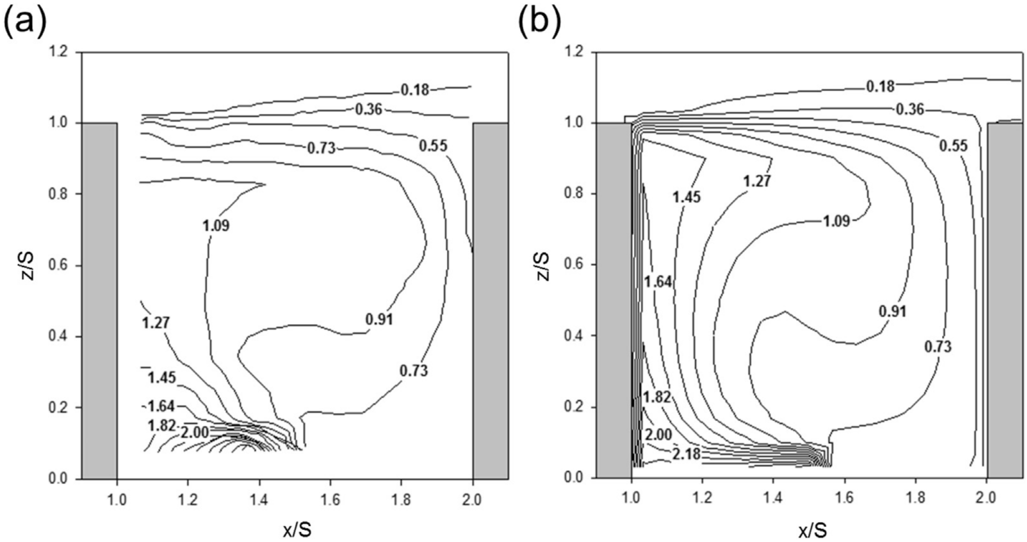

Fig. 2. Contours of nondimensionalized concentrations of pollutants (a) measured by Pavageau and Schatzmann (1999) and (b) simulated in this study.

($z/S < 0.5$), making a surface convergence region near the street-canyon center (Fig. 3b). The flow pattern of the upper layer in the H/S = 2.0 case is similar to that of the H/S = 1.0 case. However, there are marked differences in the flow pattern and wind speed of the lower layer (Fig. 3c and d). In the H/S = 2.0 case, double-eddy circulation is generated and is confined within the street canyon.

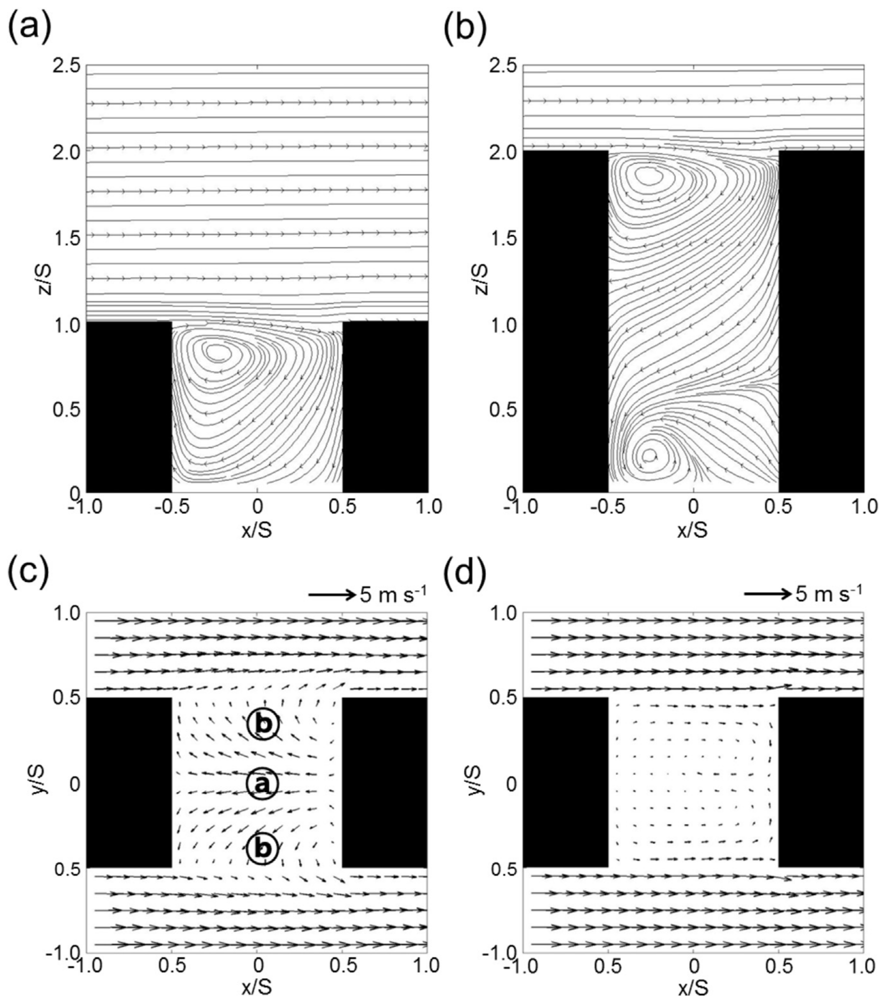

Fig. 3. Streamline fields at y/S = 0.05 [(a) and (b)] and wind vector fields at z/S = 0.15 [(c) and (d)] in the H/S = 1.0 (left panels) and H/S = 2.0 cases (right panels).

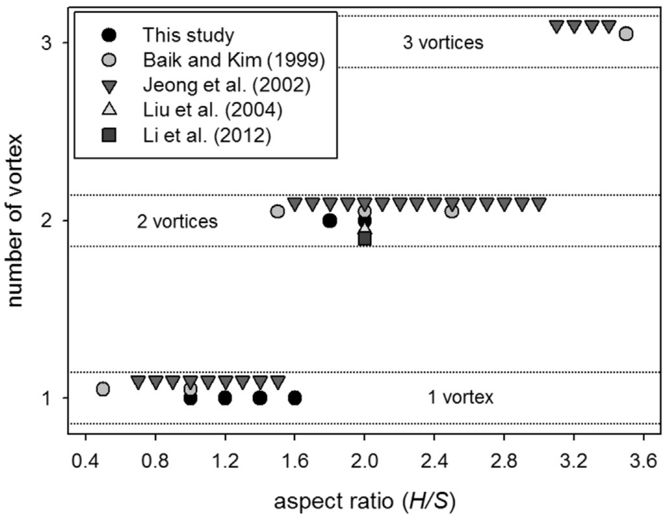

Fig. 4. Number of vortices generated in street canyons.

Wind speed at z/S = 0.15 is lower inside (1.84 and 0.77 m s^{-1} in the H/S = 1.0 and 2.0, respectively) but higher outside the street canyon than the H/S = 1.0 case (1.86 and 3.13 m s^{-1} in the H/S = 1.0 and 2.0 cases, respectively). The secondary vortex appears in a relatively deep street canyon with the aspect ratio greater than 1.6 (not shown). Previous studies on two-dimensional street-canyon flows reported that two vortices could appear in the absence of building-wall and street-bottom heating. Compared with the previous studies, two vortices are generated at a larger aspect ratio in the three-dimensional street-canyon (Fig. 4). Fig. 5 shows contours of wind components in the streamwise and vertical directions (U and W) at y/S = 0.05 in the H/S = 1.0 and 2.0 cases. In the H/S = 1.0 case, reverse and downward flows are dominant in the street canyon (Fig. 5a and c). Reverse flow is strongest near the center (Fig. 5a). Previous studies of two-dimensional street canyons have shown that upward motion is slightly weaker but appears in a wider area than downward motion to satisfy mass continuity (Huang et al., 2000; Baik and Kim, 2002; Chan et al., 2002). In the H/S = 1.0 case, upward motion is considerably weaker than downward motion (the maximum upward motion is 44.22% of the maximum downward motion) and it appears in a narrower area. In the context

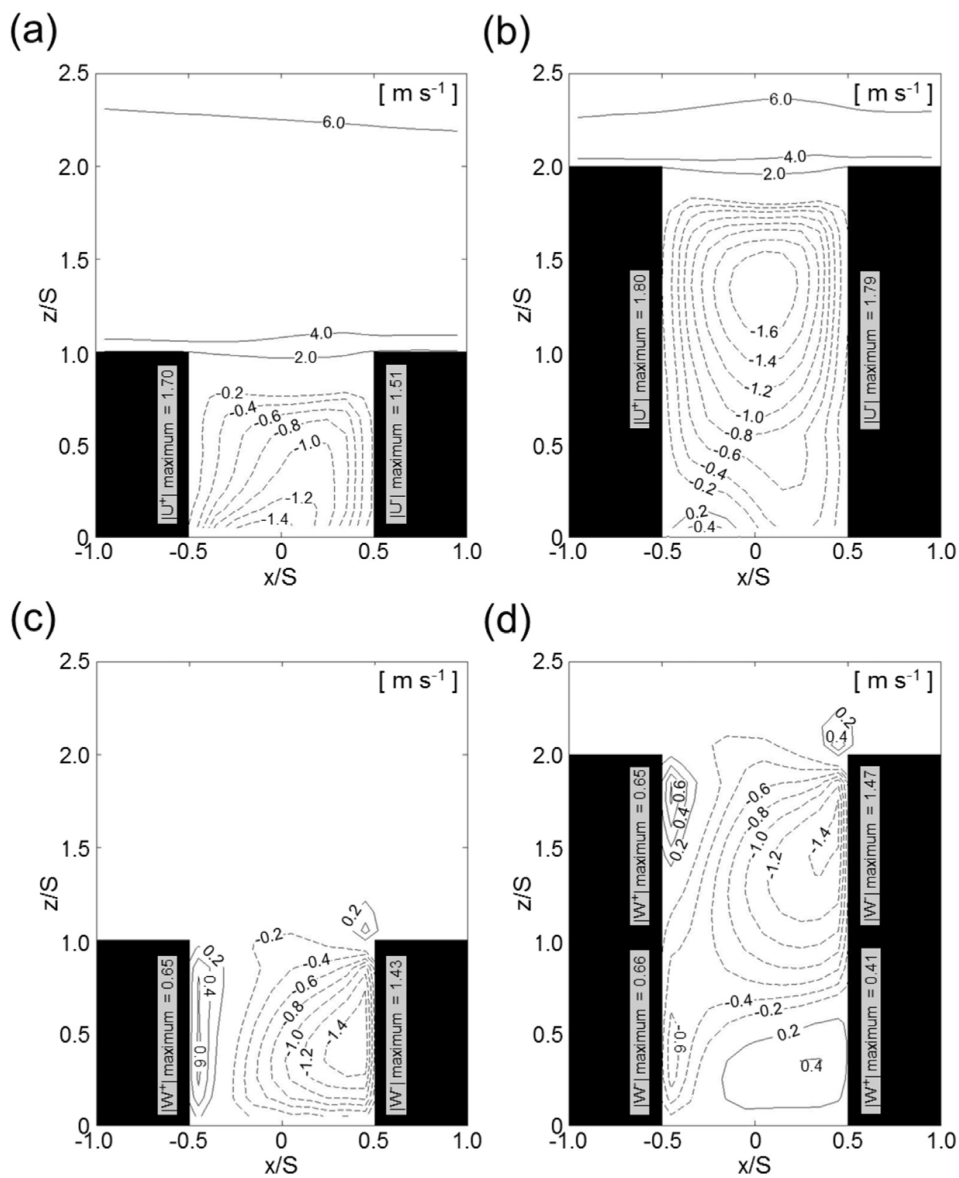

Fig. 5. Contours of U [(a) and (b)] and W components [(c) and (d)] at y/S = 0.05 in the H/S = 1.0 (left panels) and H/S = 2.0 cases (right panels).

of a mass continuity, this implies that much of the airflow originates from the streamwise street near the downwind building and escapes near the street bottom. In the H/S = 2.0 case, reverse flow is also dominant and appears in the whole street canyon, except for small areas between the upwind building and street bottom (Fig. 5b). The maximum reverse flow is stronger than the H/S = 1.0 case. The primary vortex is larger than the secondary vortex in the lower layer. As in the H/S = 1.0 case, downward motion of the primary vortex appears in a wider area and its maximum is higher than the upward motion. In the lower layer at z/S $\lesssim$0.6, upward motion is rather dominant and appears in a wider area than the downward motion. The ratio of the maximum upward to downward motions here is ~0.62, and is larger than the primary vortex in the H/S = 1.0 and 2.0 cases (0.43 and 0.44, respectively). This implies airflow supply from the streamwise street.

3.2. Dispersion characteristics of reactive pollutants

To investigate the effects of the VOC−NO_X ratio on the dispersion characteristics of reactive pollutants, six emission scenarios with different VOC−NO_X ratios are considered for street canyons with different aspect ratios. Fig. 6 shows the concentration fields of NO, NO_2, and O_3 in the H/S = 1.0 case with a VOC−NO_X ratio of 1.0. The distribution patterns of NO and NO_2 are almost symmetric about y/S = 0.0 and similar, except near the street bottom (Fig. 6a and b). NO and NO_2 concentrations (hereafter, referred as [NO] and [NO_2], respectively) in the street canyon are lower than in the streamwise street, except on both sides behind the upwind building (ⓒ and ⓓ in Fig. 6g). Although the emission ratio of NO to NO_2 is 10:1, the ratio of [NO] to [NO_2] is less than 10, which implies that NO is destroyed by reaction with O_3, generating NO_2. Near the street bottom (z/S = 0.15), a relatively high [NO] ([NO] ridge) appears along the thick line in Fig. 6a. This pattern results from the reverse and outward flow

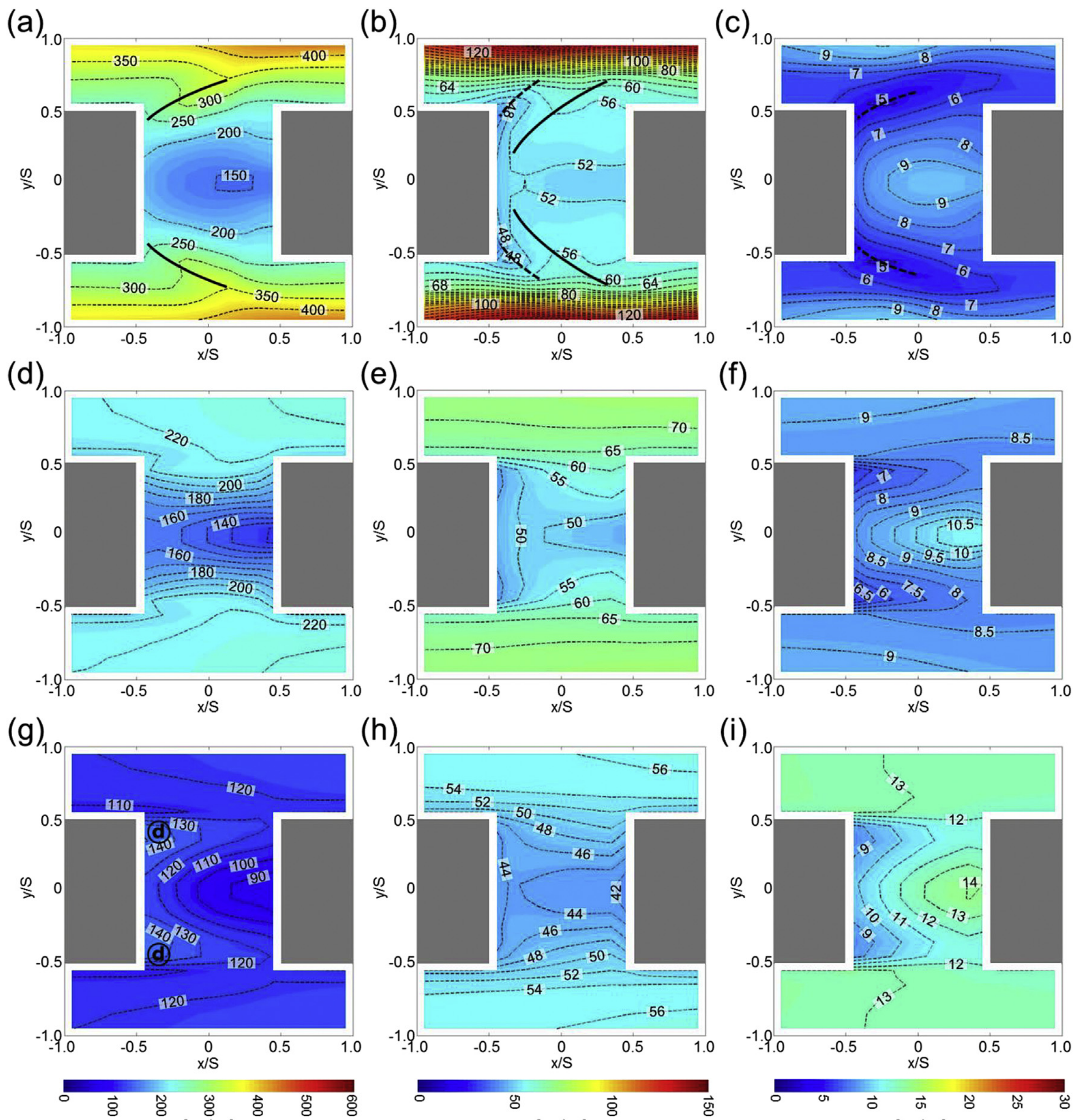

Fig. 6. Contours of [NO] (left panels), [NO_2] (middle panels), and [O_3] (right panels) at z/S = 0.15 [(a), (b), and (c)], 0.55 [(d), (e), and (f)], and 0.95 [(g), (h), and (i)] in the H/S = 1.0 case with a VOC−NO_X ratio of 1.0.

in the street canyon and the streamwise flow in the streamwise streets (ⓐ and ⓑ in Fig. 3c). Also, there is a [NO_2] trough (thick dashed line) and ridge (thick line) on both sides behind the upwind building. The minimum [NO] appears in the downwind region ($x/S = 0.25$ and $y/S = 0.0$), which is caused by airflow coming from the upper layer with relatively low [NO]. The [NO_2] distribution is similar to that of [NO] except that the minimum [NO_2] appears on both sides behind the upwind building. At the mid level of the street canyon ($z/S = 0.55$), the [NO] and [NO_2] distributions are similar to those near the street bottom, respectively, and there are saddle points at the upwind region (Fig. 6d and e). Near the roof level ($z/S = 0.95$), the minimum [NO] and [NO_2] appear near the downwind center region. [NO_2] in the street canyon is lower than in the streamwise street. However, [NO] on both sides behind the upwind building is higher than inside the streamwise street, which results from the advection of high [NO] by the upward motion. Note that the vertical gradient of [NO_2] is much smaller than that of [NO]. [NO] and [NO_2] concentrations decrease with height, while O_3 concentrations (hereafter, referred as [O_3]) increases with height. Because of NO titration, [O_3] is overall high where [NO] is low. Very low [O_3] appears near the street bottom ($z/S = 0.15$) and [O_3] near the street bottom is ~13–25% of background [O_3] (40 ppbv) (Fig. 6c). Also, relatively low [O_3] appears along the [NO] ridge, which can be referred to as the [O_3] trough (Fig. 6f). High [O_3] appears at the downwind region where airflow with high [O_3] descends. At the mid level of the street canyon ($z/S = 0.55$), the maximum [O_3] appears near the downwind center region and is higher than [O_3] in the streamwise street. [O_3] on both sides behind the upwind building is very low because the low [O_3] is advected from the lower layer by the upward motion there. Near the roof level ($z/S = 0.95$), the [O_3] and [NO] distributions are almost opposite within the street canyon. Also, it is seen that the size of the [O_3] trough decreases with height. The downward motion near the downwind building contributes to the high [O_3] in the street canyon.

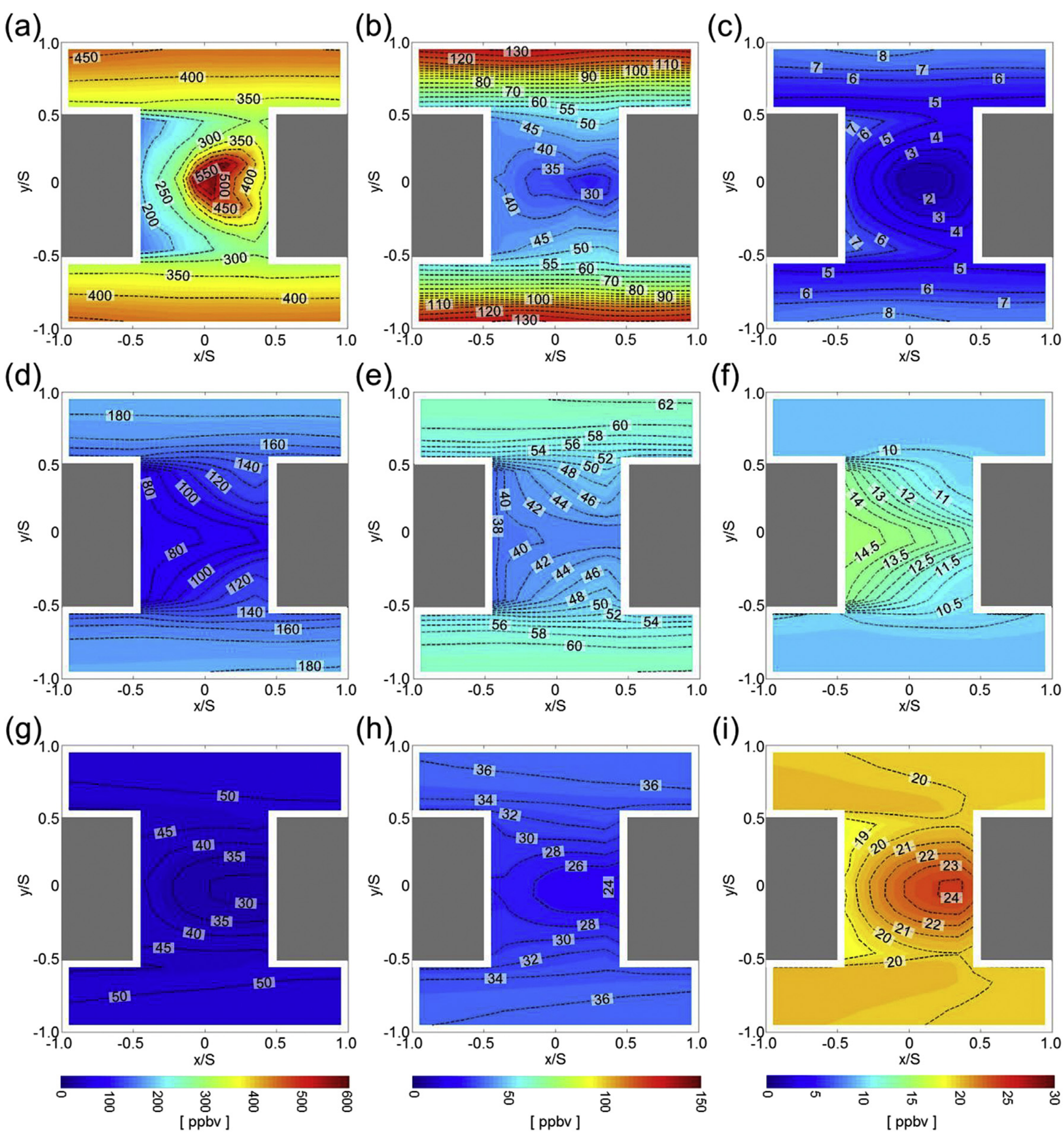

Fig. 7. Contours of [NO] (left panels), [NO_2] (middle panels), and [O_3] (right panels) at $z/S = 0.15$ [(a), (b), and (c)], 0.95 [(d), (e), and (f)], and 1.95 [(g), (h), and (i)] in the $H/S = 2.0$ case with a VOC–NO_X ratio of 1.0.

Fig. 7 shows the contours of [NO], [NO_2], and [O_3] in the H/S = 2.0 case with a VOC–NO_X ratio of 1.0. Near the street bottom (z/S = 0.15), the dispersion patterns are quite different from those in the H/S = 1.0 case. Comparing the concentrations at the same height, [NO] and [NO_2] are higher in the streamwise street, while, [O_3] in the streamwise street is lower in the H/S = 2.0 case than the H/S = 1.0 case. Near the street bottom, the maximum [NO] appears at the center of the street canyon (x/S = 0.0 and y/S = 0.0) where flow converges (Fig. 3b and d) and [NO] is higher in the downwind region (x/S > 0.0) than the upwind region (x/S < 0.0) in the street canyon (Fig. 7a). The low [NO] in the upwind region is caused by downward airflow with low [NO]. On the other hand, the minimum [NO_2] appears in the downwind region (x/S = 0.25, y/S = 0.0) and [NO_2] is lower in the downwind region than in the upwind region in the inner street canyon ($-0.25 \lesssim$ y/S $\lesssim 0.25$) (Fig. 7b). Because there are no distinct outward and reverse flows crossing the source region, the [NO] ridge and [O_3] trough are not formed in the upwind region. The relatively high [O_3] region is formed at both the sides behind the upwind building where [NO] is relatively low (Fig. 7c). At the mid level (z/S = 0.95), the [NO_2] distribution is similar to that at z/S = 0.95 in the H/S = 1 case (Fig. 7e). [NO] is high near the downwind region and [O_3] is the opposite because airflow coming from the upper layer has low [NO] and high [O_3] (Fig. 7d and f). At the roof level (z/S = 1.95), [NO] and [NO_2] are lower than those in the H/S = 1.0 case, while [O_3] is higher than those in the H/S = 1.0 case. [NO] and [NO_2] is lower in the downwind region where air flow having low [NO] and [NO_2] comes into the street canyon from the upper layer and [O_3] is the opposite.

Fig. 8 shows the contours of [NO], [NO_2], and [O_3] in the H/S = 1.0 case with the VOC–NO_X ratio of 6.0. [NO] and [NO_2] are lower than those in the VOC–NO_X ratio of 1.0 because we control the ratio by changing NO_X emission and fixing VOC emission [NO], [NO_2], [O_3] distribution patterns are similar to those in the H/S = 1.0 case with a VOC–NO_X ratio of 1.0. It also appears that [NO] and [NO_2] ridges and [NO_2] and [O_3] troughs are caused by the outward and reverse flows near the street bottom (Fig. 8a and c). The ridges

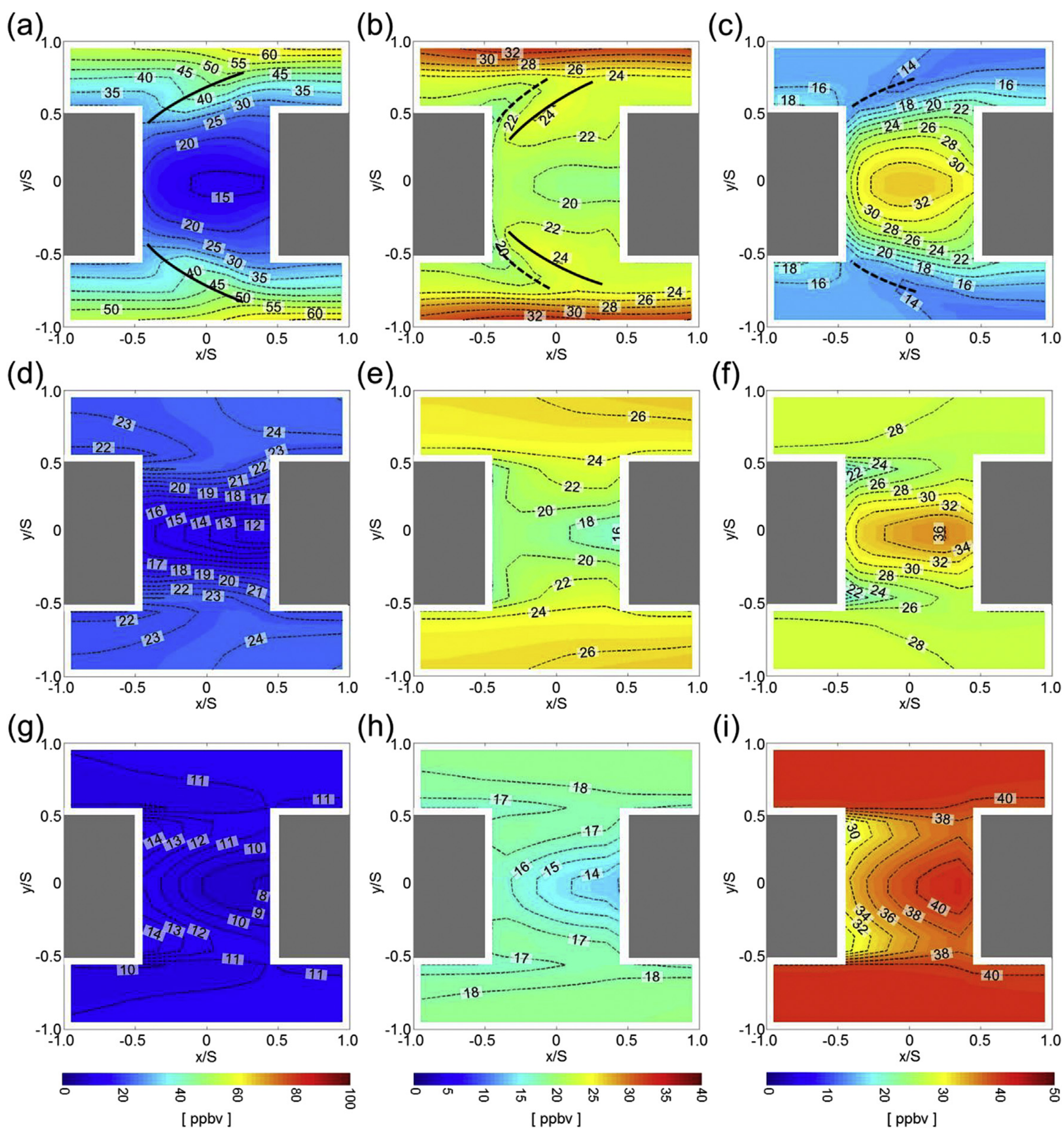

Fig. 8. The same as in Fig. 6 except for a VOC–NO_X ratio of 6.0.

and troughs reach farther downstream than the H/S = 1.0 case with the VOC–NO_X ratio of 1.0. [NO_2] is similar to [NO] in the street canyon and inner street canyon ($-0.3 < y/S < 0.3$), [NO_2] is higher than [NO]. The maximum [O_3] is 33.5 ppbv, and corresponds to 84% of the background [O_3]. Comparing the H/S = 1.0 case with a VOC–NO_X ratio of 1.0, [O_3] is less affected by [NO] titration. At the mid level (z/S = 0.55), [NO_2] is higher than [NO] even in the streamwise street. The maximum [O_3] (36.18 ppbv) appears at the downwind region and it is about threefold higher than the H/S = 1.0 case with a VOC–NO_X ratio of 1.0. Near the roof level (z/S = 0.95), [O_3] in the streamwise street and near the downwind region in the street canyon is higher than the background [O_3]. The maximum [O_3] (41.54 ppbv) appears near the downwind region (x/S = 0.35 and y/S = 0.0).

Fig. 9 shows the contours of [NO], [NO_2], and [O_3] in the H/S = 2.0 case with a VOC–NO_X ratio of 6.0. [NO_2] is higher than [NO], except near the street bottom (z/S = 0.15). A horizontal gradient of [O_3] near the street bottom is very large in the street canyon. [O_3] is high near the upwind building where relatively high [O_3] is advected from the upper layer and there is weak [NO] titration. On the other hand, strong [NO] titration results in low [O_3] in the downwind region. At z/S = 0.95, the maximum [O_3] (44.22 ppbv) appears near the upwind region in the street canyon (x/S = −0.35 and y/S = 0.0) (Fig. 9f) and [O_3] exceeds background [O_3]. The high [O_3] near the upwind region is caused by downward flow with high [O_3]. At z/S = 1.95, [O_3] in the street canyon is lower than the streamwise street because of the advection of low [O_3] by upward motion. The maximum [O_3] (46.44 ppbv) appears on both sides in front of the downwind building in the street canyon (x/S = 0.35 and y/S = ±0.45) (Fig. 9i). The formation of O_3 is related to the photolysis of NO_2. The degradation reaction of VOCs induces the formation of RO_2 and HO_2 radicals. These RO_2 and HO_2 radicals react with NO, converting NO to NO_2, which is then photolyzed to form O_3 (Sillman, 1999; Atkinson, 2000). [NO] is lower than [NO_2] at z/S = 0.95 and 1.95 in the VOC–NO_X ratio of 6.0, and it leads higher [O_3] than background [O_3]. We investigated the effect of the

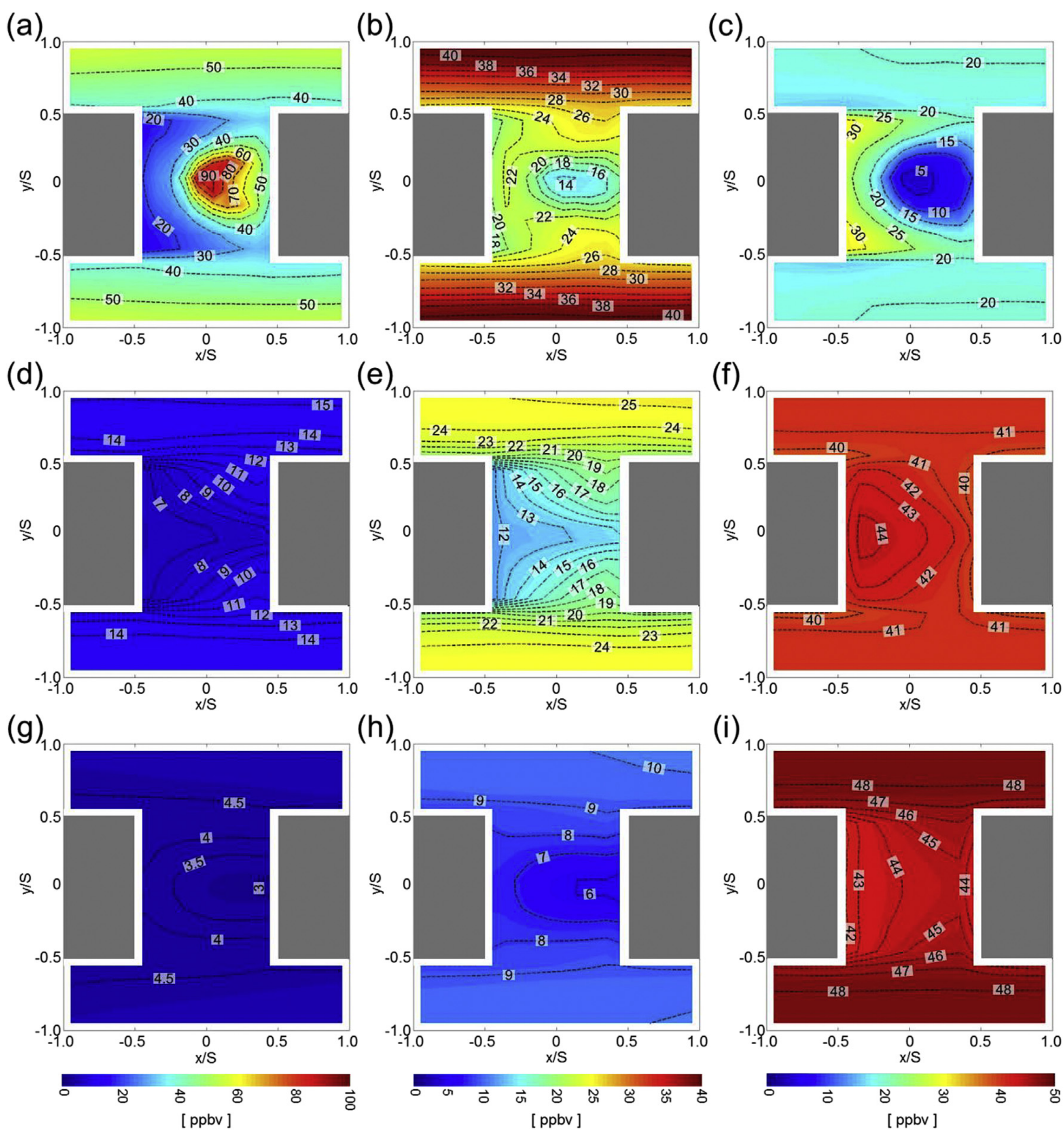

Fig. 9. The same as in Fig. 7 except for a VOC–NO_X ratio of 6.0.

street-canyon aspect ratio and VOC–NO_X ratio on [NO_X] and [O_3] in the street canyon. For this, we averaged [NO_X] and [O_3] over the whole volume (referred as $[\overline{NO_X}]$ and $[\overline{O_3}]$, respectively), upper half volume ($[\overline{NO_X}]_{up}$ and $[\overline{O_3}]_{up}$), and lower half volume of street canyons ($[\overline{NO_X}]_{dn}$ and $[\overline{O_3}]_{dn}$) and plotted them as functions of aspect ratio and VOC–NO_X ratio (Fig. 10). As the aspect ratio increases, $[\overline{NO_X}]$ decreases but $[\overline{O_3}]$ increases in shallow street canyons where one vortex is generated ($1.0 \leq H/S \leq 1.6$) for the all emission scenarios (Fig. 10a and b). This is because the outward flow becomes strong as the aspect ratio increases in shallow street canyons (Fig. 11a). The increasing outward NO_X flux from the street canyon (Fig. 11b) results in less NO titration in the street canyon. Also, we further investigated NO_X flux by mean flow and turbulence (not shown), and the results showed that NO_X flux by mean flow made a considerable contribution to outward transport of NO_X from the street canyon. In deep street canyons where two vortices are generated ($1.6 < H/S \leq 2.0$), outward flow becomes weak with the aspect ratio and outward NO_X flux decreases (Fig. 11b), resulting in

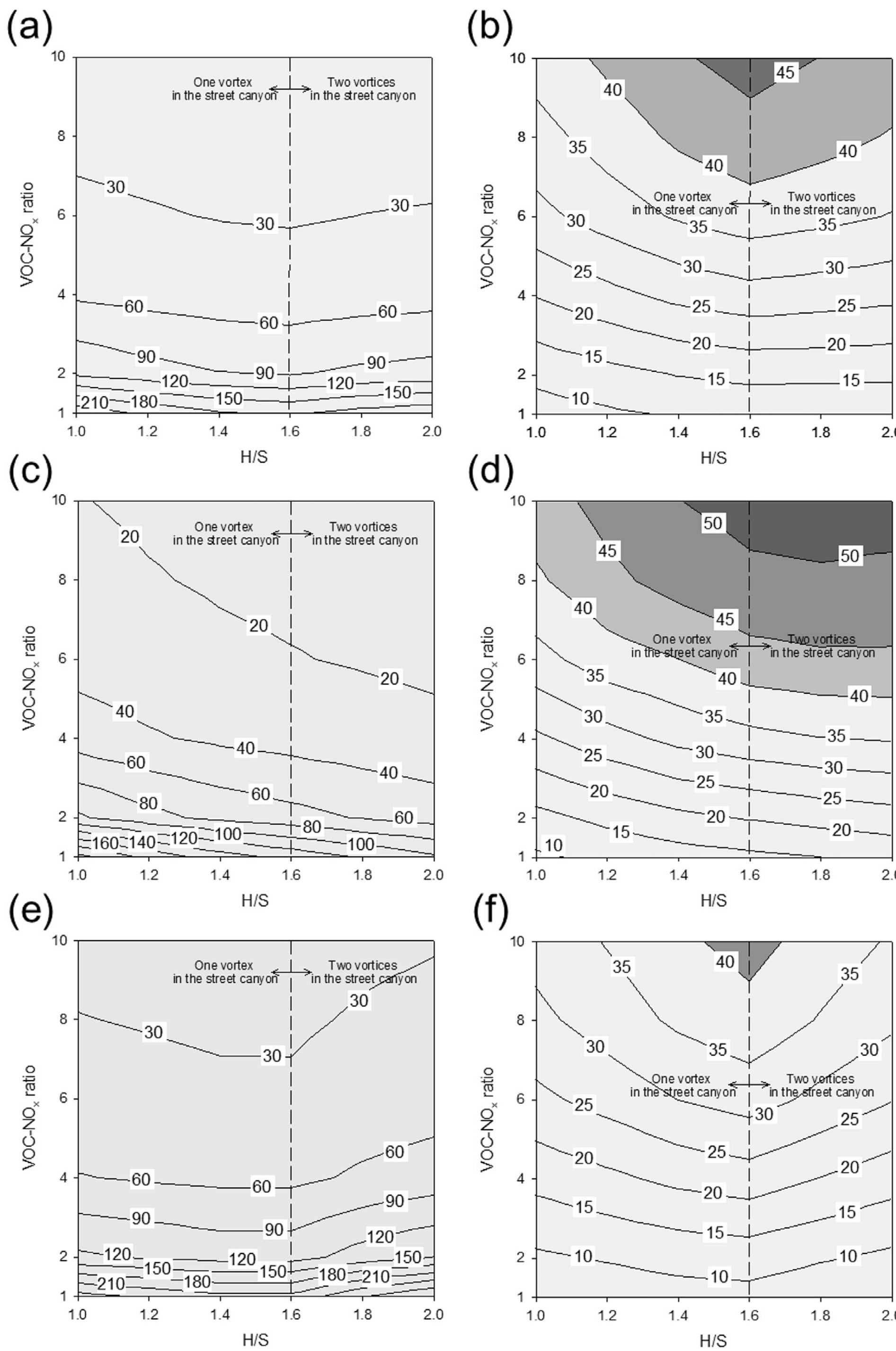

Fig. 10. Isopleth of [NO_X] (left panels) and [O_3] (right panels) averaged over the whole volume [(a) and (b)], upper half volume [(c) and (d)], and lower half volume of street canyons [(e) and (f)] in ppbv.

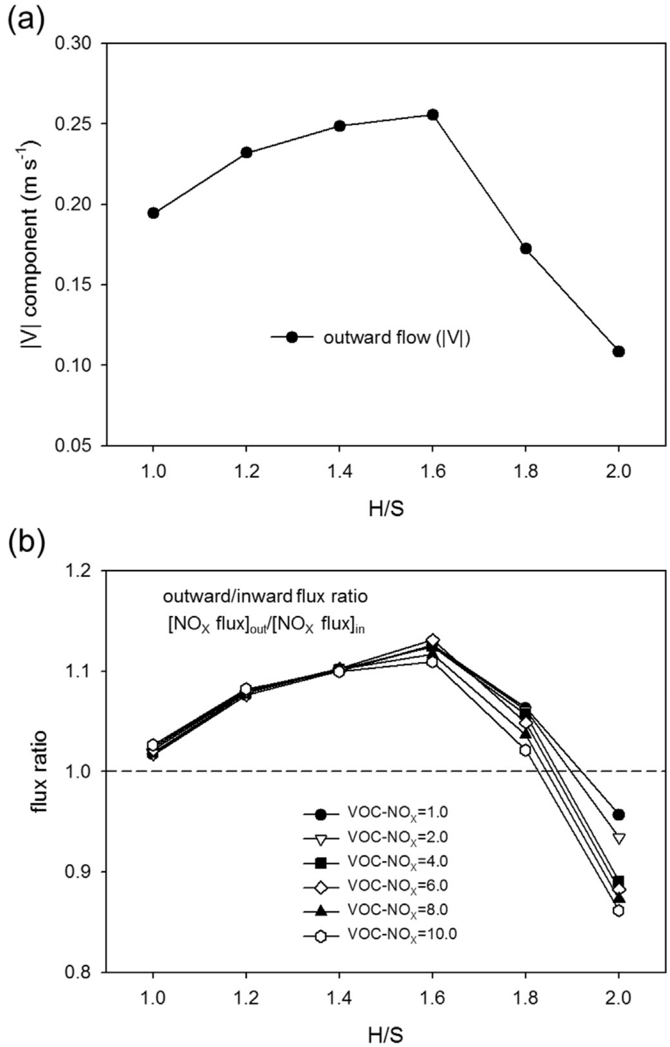

Fig. 11. The magnitude of (a) outward flow (|V|) and (b) ratio of outward to inward NO_X fluxes by mean flow averaged on the lateral (y/S = −0.5 and 0.5) and upper boundaries (roof level) of street canyon.

an increase in $[\overline{NO_X}]$ and decrease in $[\overline{O_3}]$ (Fig. 10a and b). For a given aspect ratio, $[\overline{NO_X}]$ decreases with increasing VOC–NO_X ratio, while $[\overline{O_3}]$ increases as NO titration is reduced. $[\overline{O_3}]$ in the shaded area is higher than the background due to O_3 formation resulting from photolysis of NO_2 by VOC degradation reactions (Fig. 10b).

$[\overline{NO_X}]_{up}$ consistently decreases and $[\overline{O_3}]_{up}$ increases with aspect ratio in the upper street canyons (Fig. 10c and d). Note that $[\overline{O_3}]_{up}$ is higher than the background $[O_3]$ at small aspect ratios but high VOC–NO_X ratios (shaded areas in Fig. 10d). However, despite the decreasing $[\overline{NO_X}]_{up}$ (increasing $[\overline{O_3}]_{up}$) with aspect ratio, $[\overline{NO_X}]$ and $[\overline{O_3}]$ variations are controlled by $[\overline{NO_X}]_{dn}$ and $[\overline{O_3}]_{dn}$ variations in the street canyon, respectively (Fig. 10e and f).

4. Summary and conclusion

The effects of aspect ratio, defined as the ratio of building height to street width, on the dispersion of reactive pollutants in street canyons were investigated using a coupled CFD-chemistry model. Flow characteristics of different aspect ratios were analyzed first. For each aspect ratio, six emission scenarios with different VOC–NO_X ratios (varying NO_X but fixed VOCs emission) were considered. One vortex was generated when the aspect ratio was less than 1.6 (shallow street canyon). When the aspect ratio was greater than 1.6 (deep street canyon), two vortices were formed in the street canyons. Compared to previous studies on two-dimensional street canyons, the vortex center is slanted toward the upwind building and reverse and downward flows are dominant in street canyons. Near the street bottom, there is a marked difference in flow pattern between shallow and deep street canyons. Near the street bottom, reverse and downward flows are dominant in shallow street canyons and flow convergence exists near the center of deep street canyons, which results in a large difference in the NO_X and O_3 dispersion patterns in the street canyons.

NO_X concentrations are high near the street bottom and overall decrease with height. Due to NO titration, the O_3 concentrations are low at high NO concentrations. At a low VOC–NO_X ratio, NO concentrations are sufficiently high to destroy large amount of O_3 by titration, resulting in O_3 concentrations in the street canyon that are much lower than the background concentration. At high VOC–NO_X ratios, a small amount of O_3 is destroyed by NO titration in the lower layer of the street canyons. However, in the upper layer, O_3 is formed through the photolysis of NO_2 by VOC degradation reactions. As the aspect ratio increases, the NO_X (O_3) concentration averaged over the street canyons decreases (increases) in the shallow street canyons. This is because outward flow becomes strong and NO_X flux toward the outsides of the street canyons increases, resulting in less NO titration. In the deep street canyons, outward flow becomes weak and outward NO_X flux decreases, resulting in an increase (decrease) in NO_X (O_3) concentrations.

Currently, in many countries, meso- and/or local-scale air-quality models are conducted to predict air quality in urban areas. These models cannot resolve building-scale dispersion characteristics of reactive pollutants. In particular, in the case of O_3 concentration, operating models can provide information about background O_3 concentrations. However, the street-level O_3 concentration distribution pattern is complex and concentrations differ from the background concentrations. The CFD-chemistry model can provide detailed and useful information regarding the air quality in urban areas. Considering this, we will develop a model that couples the CFD-chemistry model and WRF-CHEM or other local-scale air-quality model in the near future.

Acknowledgments

The authors are very grateful to anonymous reviewers for providing valuable comments on this work. This subject is supported by Korea Ministry of Environment as "Climate Change Correspondence Program".

References

Assimakopoulos, V.D., ApSimon, H.M., Moussiopoulos, N., 2003. A numerical study of atmospheric pollutant dispersion in different two-dimensional street canyon configurations. Atmos. Environ. 37, 4037–4049.
Atkinson, R., 2000. Atmospheric chemistry of VOCs and NO_X. Atmos. Environ. 34, 2063–2101.
Baik, J.-J., Kim, J.-J., 2002. On the escape of pollutants from urban street canyons. Atmos. Environ. 36, 527–536.
Baik, J.-J., Kang, Y.-S., Kim, J.-J., 2007. Modeling reactive pollutant dispersion in an urban street canyon. Atmos. Environ. 41, 934–949.
Baik, J.-J., Park, S.-B., Kim, J.-J., 2009. Urban flow and dispersion simulation using a CFD model coupled to a mesoscale model. J. Appl. Meteorol. Climatol. 48, 1667–1681.
Baik, J.-J., Kwak, K.-H., Park, S.-B., Ryu, Y.-H., 2012. Effects of building roof greening on air quality in street canyons. Atmos. Environ. 61, 48–55.
Baker, J., Walker, H.L., Cai, X., 2004. A study of the dispersion and transport of reactive pollutants in and above street canyons – a large eddy simulation. Atmos. Environ. 38, 6883–6892.
Bey, I., Jacob, D.J., Yantosca, R.M., Logan, J.A., Field, B.D., Fiore, A.M., Li, Q., Liu, H.Y., Mickley, L.J., Schultz, M.G., 2001. Global modeling of tropospheric chemistry

with assimilated meteorology: model description and evaluation. J. Geophys. Res. D Atmos. 106, 23073–23095.
Buckingham, C., Clewley, L., Hutchinson, D., Sadler, L., Shah, S., 1997. London Atmospheric Emissions Inventory. London Research Centre, London.
Castro, I.P., Apsley, D.D., 1997. Flow and dispersion over topography: a comparison between numerical and laboratory data for two-dimensional flow. Atmos. Environ. 31, 893–850.
Chan, T.L., Dong, G., Leung, C.W., Cheung, C.S., Hung, W.T., 2002. Validation of a two-dimensional pollutant dispersion model in an isolated street canyon. Atmos. Environ. 36, 861–872.
Chang, C.H., Meroney, R.N., 2003. Concentration and flow distributions in urban street canyons: wind tunnel and computational data. J. Wind Eng. Indust. Aerodynamics 91, 1141–1154.
Fraser, M.P., Cass, G.R., 1998. Detection of excess ammonia emissions from in-use vehicles and the implications for fine particle control. Environ. Sci. Technol. 32, 1053–1057.
Garmory, A., Kim, I.S., Britter, R.E., Mastorakos, E., 2009. Simulations of the dispersion of reactive pollutants in a street canyon, considering different chemical mechanisms and micromixing. Atmos. Environ. 43, 4670–4680.
Gowardhan, A.A., Pardyjak, E.R., Senocak, I., Brown, M., 2011. A CFD-based wind solver for an urban fast response transport and dispersion model. Environ. Fluid Mech. 11, 439–464.
Grawe, D., Cai, X.M., Harrison, R.M., 2007. Large eddy simulation of shading effects on NO_2 and O_3 concentration within an idealized street canyon. Atmos. Environ. 41, 7304–7314.
Huang, H., Akutsu, Y., Arai, M., Tamura, M., 2000. A two-dimensional air quality model in an urban street canyon: evaluation and sensitivity analysis. Atmos. Environ. 34, 689–698.
Jacobson, M.Z., Turco, R.P., 1994. SMVGEAR: a sparse-matrix, vectorized gear code for atmospheric models. Atmos. Environ. 28, 273–284.
Jeong, S.J., Andrews, M.J., 2002. Application of the κ-ε turbulence model to the high Reynolds number skimming flow field of an urban street canyon. Atmos. Environ. 36, 1137–1145.
Kang, Y.-S., Baik, J.-J., Kim, J.-J., 2008. Further studies of flow and reactive pollutant dispersion in a street canyon with bottom heating. Atmos. Environ. 42, 4964–4975.
Kim, J.-J., Baik, J.-J., 2004. A numerical study of the effects of ambient wind direction on flow and dispersion in urban street canyons using the RNG κ-ε turbulence model. Atmos. Environ. 38, 3039–3048.
Kim, J.-J., Baik, J.-J., 2010. Effects of street-bottom and building-roof heating on flow in three-dimensional street canyons. Adv. Atmos. Sci. 27, 513–527.
Kim, J.-J., Pardyjak, E., Kim, D.-Y., Han, K.-S., Kwon, B.-H., 2014. Effects of building-roof cooling on flow and air temperature in urban street canyons. Asia-Pacific J. Atmos. Sci. 50, 365–357.
Kim, M.-J., Park, R.-J., Kim, J.-J., 2012. Urban air quality modeling with full O_3–NO_X–VOC chemistry: Implications for O_3 and PM air quality in a street canyon. Atmos. Environ. 47, 330–340.
Kikumoto, H., Ooka, R., 2012. A numerical study of air pollutant dispersion with bimolecular chemical reactions in an urban street canyon using large-eddy simulation. Atmos. Environ. 54, 456–464.
Kwak, K.-H., Baik, J.-J., 2012. A CFD modeling study of the impacts of NO_X and VOC emissions on reactive pollutant dispersion in and above a street canyon. Atmos. Environ. 46, 71–80.
Liu, C.H., Barth, M.C., Leung, D.Y.C., 2004. Large-eddy simulation of flow and pollutant transport in street canyons of different building-height-to-street-width ratios. J. Appl. Meteorol. 43, 1410–1424.
Li, X.X., Britter, R.E., Norford, L.K., Koh, T.Y., Entekhabi, D., 2012. Flow and pollutant transport in urban street canyons of different aspect ratios with ground heating: large-eddy simulation. Bound. Layer Meteorol. 142, 289–204.
Meroney, R.N., Pavageau, M., Rafailidis, S., Schatzmann, M., 1996. Study of line source characteristics for 2-D physical modelling of pollutant dispersion in street canyons. J. Wind Eng. Indust. Aerodynamics 62, 37–56.
Park, S.-K., Kim, S.-D., Lee, H.-K., 2004. Dispersion characteristics of vehicle emission in an urban street canyon. Sci. Total Environ. 323, 263–271.
Pavageau, M., Schatzmann, M., 1999. Wind tunnel measurements of concentration fluctuations in an urban street canyon. Atmos. Environ. 33, 3961–3971.
Sagrado, A.P.G., van Beeck, J., Rambaud, P., Olivari, D., 2002. Numerical and experimental modelling of pollutant dispersion in a street canyon. J. Wind Eng. Indust. Aerodynamics 90, 321–339.
Schmid, H., Pucher, E., Ellinger, R., Biebl, P., Puxbaum, H., 2001. Decadal reductions of traffic emissions on a transit route in Austria – results of the Tauern tunnel experiment 1997. Atmos. Environ. 35, 3585–3593.
Sillman, S., 1999. The relation between ozone, NO_X and hydrocarbons in urban and polluted rural environments. Atmos. Environ. 33, 1821–1845.
Sini, J.F., Anquetin, S., Mestayer, P.G., 1996. Pollutant dispersion and thermal effects in urban street canyons. Atmos. Environ. 30, 2659–2677.
Tominaga, Y., Stathopoulos, T., 2010. Numerical simulation of dispersion around an isolated cubic building: model evaluation of RANS and LES. Build. Environ. 45, 2231–2239.
Uehara, K., Murakami, S., Oikawa, S., Wakwmatsu, S., 2000. Wind tunnel experiments on how thermal stratification affects flow in and above urban street canyons. Atmos. Environ. 34, 1553–1562.
Weschler, C.J., 2006. Ozone's impact on public health: contributions from indoor exposures to ozone and products of ozone-initiated chemistry. Environ. Health Perspect. 114, 1489–1496.
Xie, S., Zhang, Y., Qi, L., Tang, X., 2003. Spatial distribution of traffic-related pollutant concentrations in street canyons. Atmos. Environ. 37, 3213–3224.
Yoshie, R., Jiang, G., Shirasawa, T., Chung, J., 2011. CFD simulations of gas dispersion around high-rise building in non-isothermal boundary layer. J. Wind Eng. Indust. Aerodynamics 99, 279–288.